IEEE TRANSACTIONS ON

GEOSCIENCE AND REMOTE SENSING

A PUBLICATION OF THE IEEE GEOSCIENCE AND REMOTE SENSING SOCIETY

MARCH 2010 VOLUME 48 NUMBER 3 IGRSD2 (ISSN 0196-2892)

PART I OF TWO PARTS

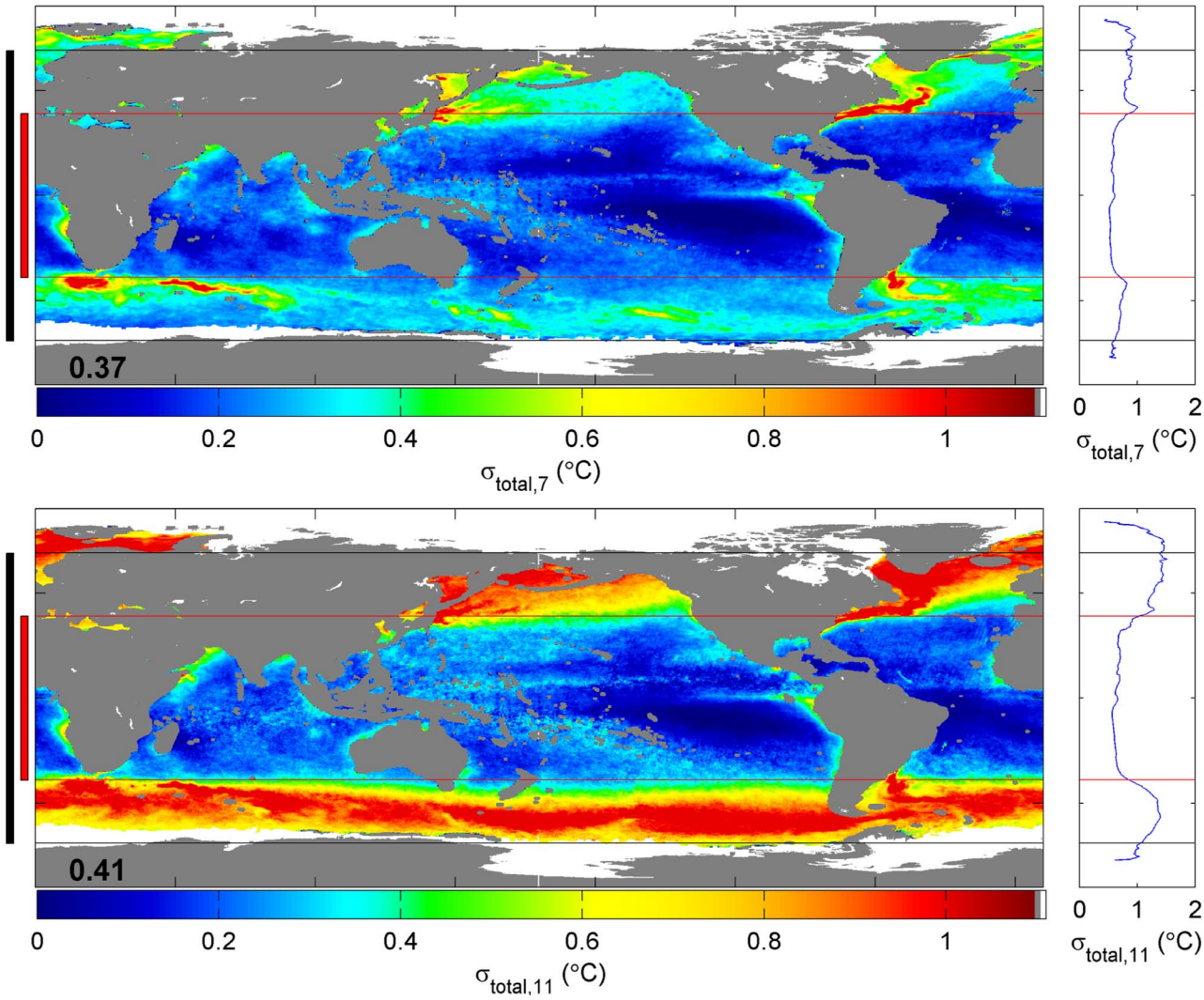

Uncertainty of SST retrievals at 7 and 11 GHz shown by the standard deviation of (top) 7-GHz AMSR-E–Reynolds SSTs and (bottom) 11-GHz AMSR-E–Reynolds SSTs. Latitudes measured by the current TRMM TMI sensor (red) and future GPM GMI sensor (black) are shown on the left. Latitudinal average standard deviation is shown on the right.

Accuracy of Satellite Sea Surface Temperatures at 7 and 11 GHz

Chelle L. Gentemann, *Member, IEEE*, Thomas Meissner, *Member, IEEE*, and Frank J. Wentz

***Abstract*—Satellite microwave radiometers capable of accurately retrieving sea surface temperature (SST) have provided great advances in oceanographic research. A number of future satellite missions are planned to carry microwave radiometers of various designs and orbits. While it is well known that the 11 GHz SST retrievals are less accurate than the 7 GHz retrievals, particularly in colder waters, it has not been demonstrated using existing microwave data. The Advanced Microwave Scanning Radiometer—Earth Observing System (AMSR-E) provides the means to examine the accuracies of SST retrievals using these channels in a systematic manner. In this paper, the accuracies of SSTs at 7 and 11 GHz are determined using two approaches: modeled and empirical. The modeled accuracies are calculated using an emissivity model and climatology SSTs, while empirical accuracies are estimated through validation of AMSR-E 7 and 11 GHz SST retrievals using over six years of data. It was found that the 7 GHz SST retrievals have less errors due to radiometer noise and geophysical errors than the 11 GHz retrievals at all latitudes. Additionally, while averaging the 11 GHz retrievals will diminish error due to uncorrelated radiometer noise, the geophysical error is still higher than for the 7 GHz retrievals, particularly at the higher latitudes.**

***Index Terms*—Advanced Microwave Scanning Radiometer—Earth Observing System (AMSR-E), microwave radiometers, sea surface temperature (SST), Tropical Rainfall Measuring Mission Microwave Imager (TMI).**

I. Introduction

SEA-SURFACE temperatures (SSTs) from satellites carrying microwave radiometers have been continuously available since December 1997 when the Tropical Rainfall Measuring Mission (TRMM) Microwave Imager (TMI) was launched. Microwave "through-cloud" SST retrievals have become a mainstay for ocean research as they provide an uninterrupted view of the ocean surface, free of cloud and water vapor contamination [1], [2]. Areas of active rain do have to be excluded, but they are easily identified and removed. The number of peer-reviewed papers shows that microwave SSTs play an important role in Earth science research [3]–[8].

Two joint Japanese Aerospace Exploration Agency and National Aeronautics and Space Administration (NASA) satellite microwave radiometers currently retrieved SST: the previously mentioned TMI and the Aqua satellite, launched May 4, 2002, carrying the Advanced Microwave Scanning Radiometer—Earth Observing System (AMSR-E) microwave radiometer. TMI is a sun-asynchronous satellite in a low-inclination orbit, retrieving data within 40° N−S [9]. It has nine channels, corresponding to five frequencies (11, 19, 21, 37, and 85 GHz) and two polarizations (vertical and horizontal) in all but the 21 GHz. SST retrieval spatial resolution is determined by the 11 GHz field of view, 59 × 36 km. AMSR-E has 12 channels corresponding to six frequencies (7, 11, 19, 24, 37, and 85 GHz) and two polarizations (vertical and horizontal). The field of view for the 7 GHz horn is 76 × 44 km, and that for the 11 GHz horn is 49 × 28 km, setting the SST retrieval spatial resolutions. Both TMI and AMSR-E are conical scanning radiometers, viewing the Earth at a constant incidence angle of approximately 55°. This is the first polar orbiting microwave radiometer capable of accurate global SSTs since the poorly calibrated Scanning Multichannel Microwave Radiometer (SMMR) was launched in 1978 [2]. The SST retrieval algorithm used for both TMI and AMSR-E is described in Section II-A.

Future radiometers on planned satellite missions are the Global Climate Observation Mission—Weather (GCOM-W) AMSR2 with launch scheduled for February 2011, the Global Precipitation Mission Microwave Imager (GMI), with launch scheduled for July 2013, and the National Polar Orbiting Earth System of Systems (NPOESS) Microwave Imager Scanner (MIS) with scheduled launch in 2016. The GCOM-W AMSR2 is an improved AMSR-E, having the same channels as AMSR-E, from 7 to 89 GHz but an improved hot load design. The GMI is a follow-on to the TMI, having both a similar sun-asynchronous high-inclination orbit of 60° and channels from 11 to 89 GHz. NPOESS MIS is planned to measure from 7 to 89 GHz (AMSR-E's channels), but will have additional channels at 50–60, 150, and 183 GHz (used primarily for atmospheric sounding). Since future planned microwave radiometers have various orbit inclinations and retrieval channels, it is important to understand how this may impact SST retrieval accuracy.

II. Data and Algorithm Description

As stated previously, the AMSR-E has 12 channels corresponding to six frequencies (7, 11, 19, 24, 37, and 85 GHz) and two polarizations (vertical and horizontal). Since May 2002, it has been orbiting at an altitude of 705 km, with a 1.6 m antenna, resulting in a swath width of 1450 km and surface footprint of 44–76 km. The AMSR-E data are ideal for examining the accuracy of SSTs from retrieval algorithms using different combinations of the channels.

Manuscript received February 12, 2009; revised April 29, 2009 and June 17, 2009. First published October 30, 2009; current version published February 24, 2010. This work was supported by the National Aeronautics and Space Administration Physical Oceanography Program Manager Eric Lindstrom under Grant NNH08CC60C.

The authors are with Remote Sensing Systems, Santa Rosa, CA 95401 USA (e-mail: gentemann@remss.com; meissner@.com; frank.wentz@remss.com).

Digital Object Identifier 10.1109/TGRS.2009.2030322

A. SST Retrieval Algorithm

The vertically polarized brightness temperature (T_B) of the ocean surface is sensitive to SST between 4 and 11 GHz [10]. T_B also depends on the sea surface roughness and intervening atmospheric temperature and moisture profile. Fortunately, the spectral and polarimetric signatures of the surface roughness and intervening atmosphere are quite distinct from the SST signature, and the influence of these effects can be removed, given simultaneous measurements at multiple frequencies and polarizations.

The algorithm regression coefficients are found by generating a large ensemble of simulated T_B computed from a microwave radiative transfer model (RTM) for the ocean and intervening atmosphere [11]. The simulation is based on a set of 42 195 radiosonde soundings launched from weather ships and small islands around the globe [12]. These data are used to specify the atmospheric part of the RTM. For each radiosonde, a large range of sea surface conditions is considered. The sea surface wind speed is varied from 0 to 40 $\mathrm{m \cdot s^{-1}}$, and the wind direction is varied over the full 360° range. The SST is varied by ± 5.5 °C about the Reynolds SST (described in Section II-B) for the island site. For each of these Earth scenes, the RTM computes the full set of AMSR-E T_B with a realistic sensor noise of 0.1 K added. This data set then consists of known ocean and atmospheric parameters and simulated AMSR-E data.

The AMSR-E SST retrieval algorithm is a physically based regression that expresses SST in terms of T_B. The algorithm operates in two stages. In the first stage, initial estimates of SST and wind speed are obtained via a summation over all the AMSR-E channels using regression coefficients that were determined from an RTM, as discussed previously. The first-guess SST provides a reasonably good initial estimate. However, the relationship of T_B versus SST and wind is nonlinear, and the simple summation is not capable of fully representing these nonlinearities. Hence, we add a second stage to the retrieval algorithm. For the second stage, a large set of localized retrieval algorithms is used. By "localized," we mean that the algorithm is trained to perform well over a relatively narrow range of SST and wind speeds. Localized algorithms are derived for 38 SST reference values ranging from -3 °C to 34 °C and for 38 wind speed reference values ranging from 0 to 37 $\mathrm{m \cdot s^{-1}}$. All SST/wind combinations are considered, thereby giving a total of 1444 localized algorithms. Each algorithm is trained to perform well over an SST/wind range of ± 1.5 °C and ± 2 $\mathrm{m \cdot s^{-1}}$ centered on the reference SST and wind value. The reason for using such a large number of algorithms is to ensure good continuity in the retrievals when moving from one set of reference SST/wind to the next. The second-stage retrieval is found from a linear interpolation of the localized algorithms that are in the neighborhood of the first-stage retrievals.

For this study, two SST retrieval algorithms were developed for AMSR-E data, one regression developed using AMSR-E channels 7–37 GHz, hereafter referred to as the 7 GHz SST retrieval, and another using AMSR-E channels 11–37 GHz, hereafter referred to as the 11 GHz SST retrieval. The first algorithm is identical to the current AMSR-E operational SST algorithm (and future GCOM-W AMSR2), while the second is similar to the TMI operational SST algorithm (and future GMI). The AMSR-E T_B values are resampled to the 7 GHz channel footprint prior to calculating SSTs. The 7 and 11 GHz feedhorns are pointed in a slightly different direction than the 19–37 GHz horns, resulting in different footprint locations. The resampling 7 and 11 GHz observations match the 19 GHz footprint location. The accuracy of these two algorithms was examined using the independent infrared (IR) SST data described next.

B. IR SST Data Used for Validation

Two data sets of IR SSTs were obtained for validation and are described in the following. The Advanced Very High Resolution Radiometer (AVHRR)-only Reynolds Optimum Interpolated (OI) SST version 2.0 [13] is a daily global 25 km gridded "bulk" SST analysis produced from satellite IR and *in situ* SSTs, hereafter referred to as Reynolds SST. The satellite SSTs are from the National Oceanographic Atmospheric Administration (NOAA)'s polar orbiting satellites which carry the AVHRR onboard. Satellite data are processed using the AVHRR Oceans Pathfinder SST algorithm [14], based on the nonlinear SST algorithm developed by Walton [15]. The monthly algorithm coefficients are determined through a least-squares regression of the satellite radiances to collocated *in situ* SST measurements, with separate coefficients determined for low and high channel 4 minus channel 5 differences. The *in situ* SST measurements used in the Reynolds OI analysis are distributed by the global telecommunication system and obtained from volunteer observing ships, drifters, and moored buoys. These *in situ* data are used to correct for any large-scale satellite biases before interpolation of the satellite SSTs. The OI method utilizes estimates of retrieval error. In this application, the daytime and nighttime AVHRR retrievals are given an equal error. The analysis is produced in near real time and is available from 1981 to present. The OI method requires specification of zonal and meridional spatial scales, set to 151 km (zonal) and 155 km (meridional). In comparison, the weekly 100 km Reynolds OI SST version 1 used 859 km (zonal) and 608 km (meridional). The analysis is run using data within 400 km and three days of the grid location and time. The temporal and spatial gridding, daily and 25 km, is not necessarily the spatial resolution of the analyzed SSTs, as shown in [13].

An additional daily OI SST analysis is being produced by Reynolds, which uses the AMSR-E data [13]. The data used here to validate the AMSR-E SST retrievals are the AVHRR-only Reynolds OI SSTs.

The Pathfinder (PF) and Erosion monthly climatology [16] is a monthly 9.28 km SST climatology created from the 1985–1997 PF AVHRR SSTs. This climatology uses the day and night PF AVHRR SSTs versions 4.0, 4.1, and 4.1 interim. The PF SST algorithm uses a modified nonlinear SST algorithm originally developed by Walton [15]. The modification accounts for temporal sensor calibration drift and errors due to atmospheric water vapor by using two sets of temporally varying algorithm coefficients as described in [17]. The climatology was constructed using these SST data, but to maintain the highest quality data, valid SST data adjacent to clouds were

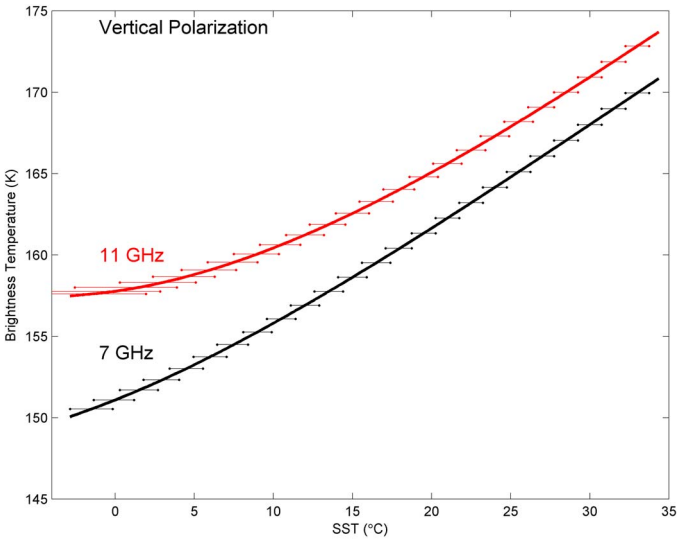

Fig. 1. Relationship between 7 and 11 GHz (vertical polarization) and SSTs. The horizontal lines show the error in SST due to 0.5 K noise in brightness temperature. For AMSR-E, the actual noise is 0.1 K, but this larger value was used to better illustrate the increase in error. The sensitivity of SST to changes in TB decreases for 11 GHz at lower SSTs, resulting in larger errors and a small positive bias (Table II).

excluded. Missing data in the monthly climatology were filled in using Gaussian interpolation. In this paper, we averaged the monthly 9.28 km climatologies to a single 25 km SST climatology; these data are hereafter referred to as the PF climatology.

III. Retrieval Error

The total error σ_{total} for a given microwave retrieval algorithm using frequency f is

$$\sigma_{\text{total,f}} = \sigma_{\text{noise,f}} + \sigma_{\text{retrieval,f}} + \sigma_{\text{collocation}} + \sigma_{\text{data}} \quad (1)$$

where the uncorrelated radiometer noise in each channel results in an error in the retrieved SST σ_{noise}. This error is nonlinear and depends on the Earth scene. Errors due to the environmental scene $\sigma_{\text{retrieval}}$ occur because accuracy decreases with increasing cloud water, wind speed, and water vapor or subpixel geophysical variability. When a validation data set is used, the total error will also include errors due to the collocation $\sigma_{\text{collocation}}$ and errors in the independent data set used for validation σ_{data}.

The accuracies of the 7 and 11 GHz SST retrievals are investigated using two methods: modeled determination of σ_{noise} and empirical errors from validation of actual SST retrievals against independent SST data. Modeled σ_{noise} is estimated from an emissivity model, where the sensitivity of the brightness temperature to SST is examined. Realistic radiometer noise is added to the brightness temperatures to demonstrate how this impacts errors in SST. Essentially, this method is a modeled estimate of σ_{noise}. An empirical estimate of σ_{total} is determined from AMSR-E validation results, and this is compared to the modeled estimate of σ_{noise}. In the following section, we first present the modeled error followed by comparisons of real-world AMSR-E validation to verify these results.

TABLE I
Sensitivity of 7 and 11 GHz Vertical Polarization Measurements to SST

SST (°C)	Sensitivity to SST (K °C^{-1})	
	7 GHz	11 GHz
0.00	0.39	0.14
15.00	0.59	0.47
30.00	0.65	0.63

TABLE II
Error in SST Due to 0.1 K Noise in Brightness Temperature at 7 and 11 GHz (Vertical Polarization). The Errors Are Approximately Equal Above 19 °C, but Below That, the 11 GHz Error Is Always Larger Than the 7 GHz Error, Increasing From 0.20 °C to 0.96 °C

SST (°C)	SST STD error		SST bias	
	7 GHz	11 GHz	7 GHz	11 GHz
-1.00	0.28	0.96	0.00	0.13
0.00	0.26	0.75	0.00	0.09
1.00	0.25	0.61	0.00	0.05
2.00	0.24	0.53	0.00	0.04
3.00	0.23	0.46	0.00	0.03
4.00	0.22	0.41	0.00	0.02
5.00	0.21	0.37	0.00	0.02
6.00	0.20	0.34	0.00	0.02
7.00	0.20	0.31	0.00	0.02
8.00	0.19	0.30	0.00	0.01
9.00	0.19	0.28	0.00	0.01
10.00	0.18	0.27	0.00	0.01
11.00	0.18	0.26	0.00	0.01
12.00	0.18	0.24	0.00	0.01
13.00	0.18	0.23	0.00	0.00
14.00	0.17	0.22	0.00	0.00
15.00	0.17	0.22	0.00	0.00
16.00	0.17	0.20	0.00	0.00
17.00	0.17	0.20	0.00	0.00
18.00	0.16	0.20	0.00	0.00
19.00	0.16	0.19	0.00	0.00
20.00	0.16	0.19	0.00	0.00
21.00	0.16	0.18	0.00	0.00
22.00	0.16	0.18	0.00	0.00
23.00	0.16	0.18	0.00	0.00
24.00	0.16	0.17	0.00	0.00
25.00	0.16	0.17	0.00	0.00
26.00	0.16	0.17	0.00	0.00
27.00	0.16	0.16	0.00	0.00
28.00	0.15	0.16	0.00	0.00
29.00	0.15	0.16	0.00	0.00
30.00	0.15	0.16	0.00	0.00
31.00	0.15	0.16	0.00	0.00
32.00	0.15	0.16	0.00	0.00
33.00	0.15	0.16	0.00	0.00
34.00	0.15	0.16	0.00	0.00

IV. Results

A. Modeled Estimate of σ_{noise}

The specular sea surface emissivity E_0 depends on SST, sea surface salinity, and emission angle. Fig. 1 shows $E_0 \cdot T_S$ (in kelvins), which is the T_B emitted from a specular ocean surface, as a function of SST (in degrees Celsius). The computation was done for vertical and horizontal polarizations at 7.0 and 11.0 GHz, respectively. E_0 was computed from the Fresnel equations [18] using the model for the dielectric constant (permittivity) of sea water by Meissner and Wentz [19], for an emission angle equal to the AMSR-E instrument angle of 55° and a sea surface salinity that is typical of the global ocean, i.e., 35 psu. The sensitivity of T_B to SST shown in Fig. 1 is also

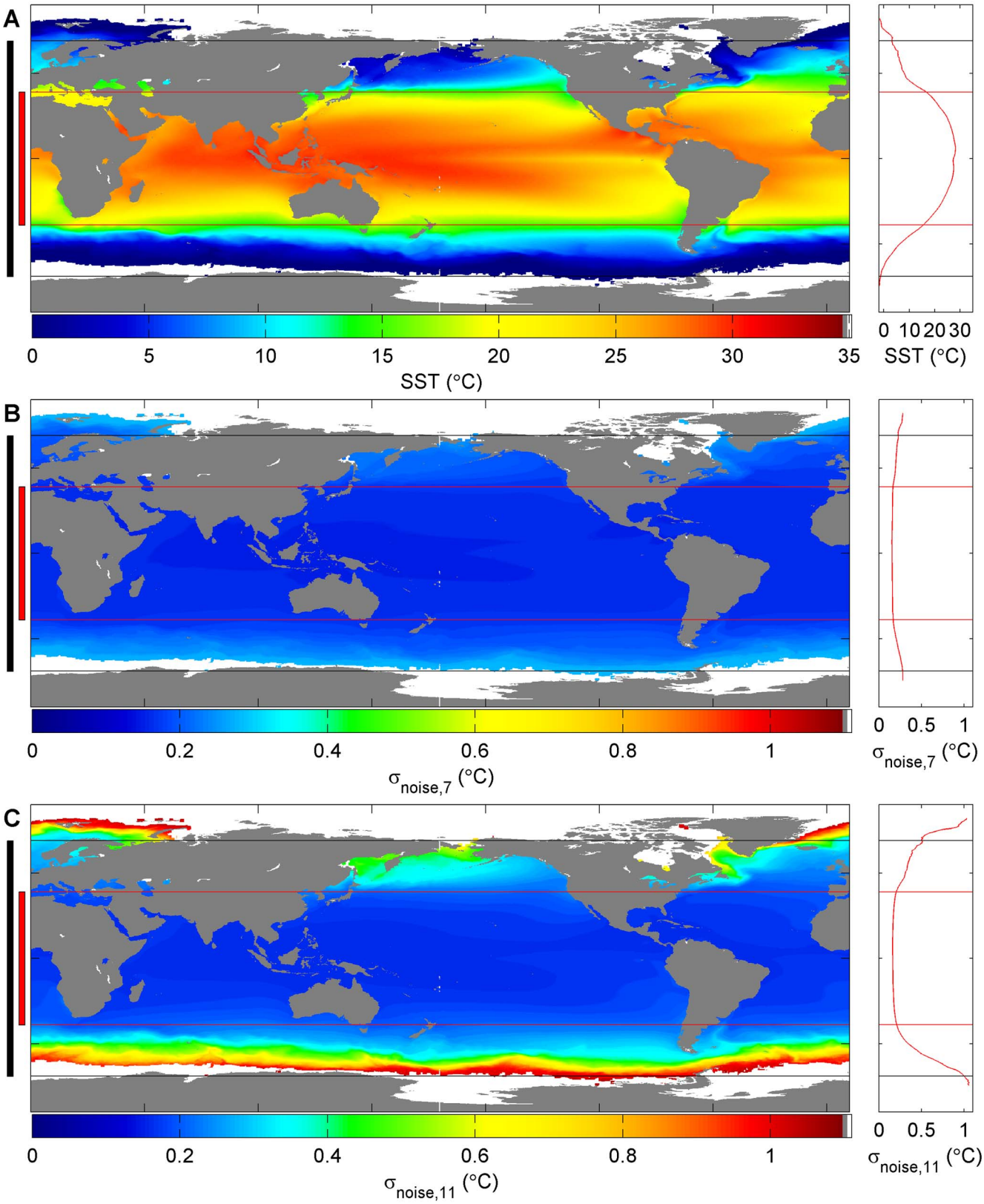

Fig. 2. Sensitivity of SST error due to radiometer noise. The latitudes measured by (red) TMI and (black) GMI are shown on the left side of each panel. The latitudinal average is shown to the right of the panels. (a) PF Climatology SST. (b) Noise error for SST retrievals at 7 GHz. (c) Noise error for SST retrievals using 11 GHz. Above 40° N−S, the SST retrievals will have an increased error due to the decreased sensitivity.

given in Table I. The 7 GHz channel has twice the sensitivity of the 11 GHz channel at 0.0 °C SST. Shibata [20], [21] showed similar results using the Klein and Swift dielectric model [22] to determine the sensitivity of SST at 4 and 10 GHz. His results are different due to both the dielectric model and frequencies. The frequencies, given in Table I, better match existing radiometer

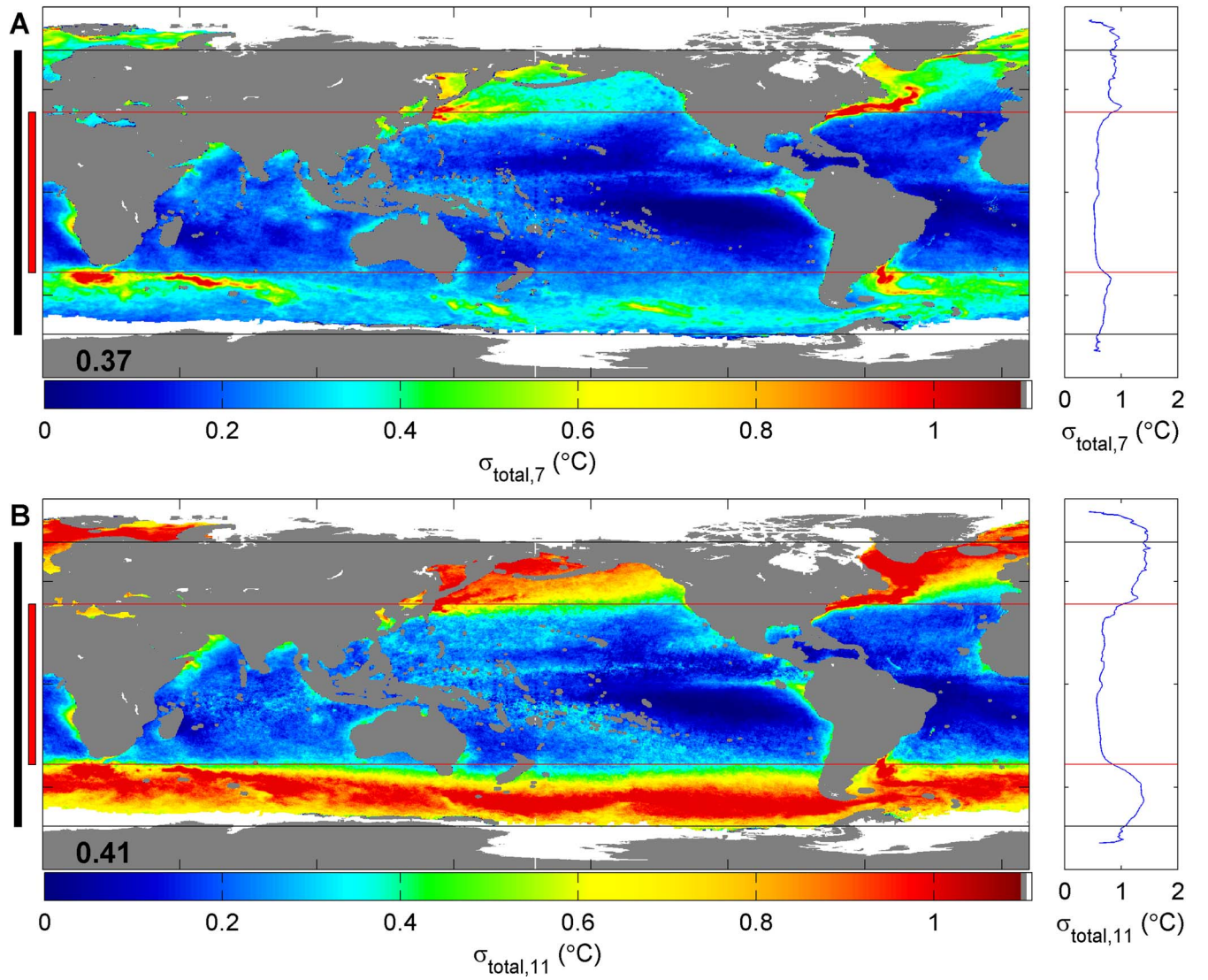

Fig. 3. Standard deviation of AMSR-E minus Reynolds SST for the (a) 7 GHz AMSR-E SSTs and (b) 11 GHz AMSR-E SSTs. The latitudes measured by (red) TMI and (black) GMI are shown on the left side of each panel. The latitudinal average is shown to the right of the panels. An estimate of the collocation error (0.37 and 0.41 K) given in the lower left corner was subtracted from each image.

configurations. The AMSR-E instrument has noise of 0.1 K [11]. Errors in SST due to radiometer noise are given in Table II and shown in Fig. 1 by the horizontal lines.[1] Above 19 °C, both channels are approximately equally sensitive to SST, but below 19 °C, the 11 GHz channel has decreased sensitivity, and Fig. 1 shows the increased error by the widening of the horizontal error lines. For 0.1 K noise, the SST error is approximately 0.2 °C. The 7 GHz SST error doubles to 0.28 °C below −1.0 °C. For the 11 GHz channel, the error increases, reaching 0.96 °C at −1.0 °C. These results indicate that, at SSTs below 19 °C, the 7 GHz retrievals will have less error. Table II also shows the positive bias at 11 GHz, below 12 °C, introduced by a non-Gaussian radiometer noise distribution due to the decreasing sensitivity.

The geographical distribution of the modeled errors was determined using the PF climatology SST data set [Fig. 2(a)]. The latitudinal region covered by TMI and GMI is shown by red and black lines, respectively. The climatological SSTs range from 15 °C to 28 °C in the region measured by TMI, 40° N−S, and from −1 °C to 28 °C in the region measured by GMI, 65° N−S. Fig. 2(b) shows the modeled error for the 7 GHz SST retrieval using data from Table II. Error increases slightly above 40° N−S. Fig. 2(c) shows the modeled error for the 11 GHz SST retrieval. Errors due to radiometer noise increase from 0.16 to 0.43 °C at 65° N and 0.87 °C at 65° S. The modeled errors show that the 7 GHz SST retrieval is valid globally while the 11 GHz SST retrieval will have a significant contribution of its error due to radiometer noise beyond 40° N−S, limiting the usefulness of the data. This effect could be somewhat minimized by using 11 GHz SST data averaged into weekly or monthly maps where the uncorrelated errors due to radiometer noise would be diminished, but this will also minimize its usefulness for research requiring subweekly or monthly variability which can be significant.

[1]The lines in Fig. 1 are plotted for a 0.5 K noise level to facilitate viewing.

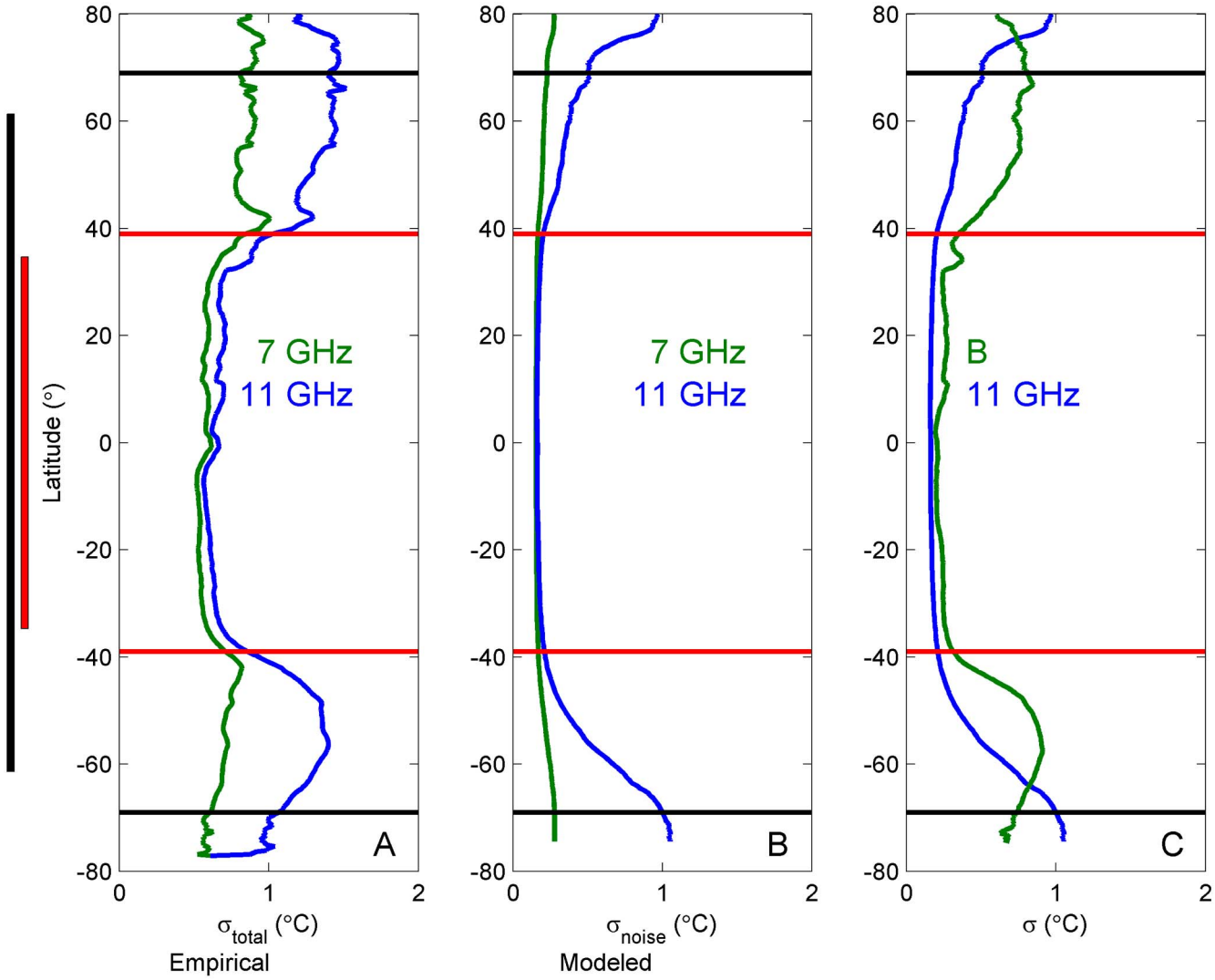

Fig. 4. Latitudinal average standard deviation for (a) the data (AMSR-E minus Reynolds SST), (b) the model (error from Table II and climatology SST), and (c) the (blue) 11 GHz model and B [from (2)], defined as the 11 GHz error plus the difference in retrieval error (11 minus 7 GHz). The latitudes measured by (red) TMI and (black) GMI are shown on the left side of each panel.

B. Empirical Estimate of σ_{noise}

To examine whether the errors due to decreased sensitivity in the 11 GHz channel are apparent in actual SST retrievals, we used Reynolds SSTs linearly interpolated in time to match the AMSR-E data which were processed using both the 7 and 11 GHz SST retrieval algorithms. Identical rain, sun glitter, and side-lobe contamination flags were used to exclude data for both SST retrieval algorithms. Collocated data from June 1, 2002 to December 31, 2008 were used to determine the SST error. Since wind speed, water vapor, cloud liquid water, and rain rates are simultaneously determined from the AMSR-E observations, these data are used to determine how the retrieval errors depend on oceanic and atmospheric parameters.

The global standard deviation of AMSR-E minus Reynolds SST is shown in Fig. 3. Similar to Fig. 2, the TMI and GMI measurement areas are shown both on the left of the figures and by lines at the corresponding latitudes. The right panel shows the mean error by latitude. As discussed previously, the error calculated in this manner will include error due to radiometer noise, retrieval error, collocation error, and errors in the Reynolds SST. The comparison between a 25 km satellite SST retrieval and the 25 km (gridded resolution) daily averaged Reynolds has a collocation error $\sigma_{\mathrm{collocation}}$ due to temporal and spatial smoothing in the analyzed SSTs. If we assume that $\sigma_{\mathrm{collocation}}$ can be globally approximated by a single number, we can estimate $\sigma_{\mathrm{collocation}}$ by forcing the difference in the modeled and empirical errors in tropical regions, where σ_{noise} is minimal, to be zero. Fig. 3(a) and (b) shows the assumed $\sigma_{\mathrm{collocation}}$ (0.37 and 0.41) in the lower left corner of each panel.

The 7 GHz retrievals [Fig. 3(a)] show the least error in the tropics, increasing toward the polar regions. The σ_{data} errors are visible in regions where there are narrow currents such as the Kuroshio Current, Gulf Stream Current, Agulhas Current, Brazil–Malvinas confluence region, and South Equatorial Countercurrent in the Pacific and in regions with strong wind-driven SST jets such as Somalia and the Gulf of Tehuantepec. These currents are temporally and spatially highly variable and are not well resolved by the Reynolds analysis used for

comparison [1]. These features disappear in comparisons between AMSR-E and high-resolution IR SST data, but we have chosen to use the Reynolds SST here because of its high-quality globally gap-filled data. The 11 GHz [Fig. 3(b)] and 7 GHz errors have a similar magnitude and spatial structure in the tropical regions, but above 40° N−S, the error increases significantly in the 11 GHz retrievals.

The latitudinal average errors for the data [Fig. 4(a)] and the model using climatological SST [Fig. 4(b)] clearly show the increase in error above 40° N−S for the 11 GHz retrievals. The data show an increase in error in both the 7 and 11 GHz retrievals at approximately 40° N−S, but Fig. 3 showed that this effect is due to the high SST variability in western boundary current regions. The sensitivity model using PF climatology SST [Fig. 4(b)] does not show the strong increase at the latitudes of the western boundary currents since the error only depends on SST, not collocations of SST. The model shows similar errors at latitudes less than 40° N−S, and the 11 GHz error increases quickly above 40° N−S. Unlike the data, the model does not show a reduction in error at the highest latitudes. To further explore this, Fig. 4(c) shows $\sigma_{\mathrm{noise},11}$ (blue) from the modeled estimate. To compare the modeled and empirical $\sigma_{\mathrm{noise},11}$, we remove the errors due to collocation and the errors in the Reynolds data as follows. Using (1), we take the difference of empirical 11 GHz errors minus empirical 7 GHz errors plus $\sigma_{\mathrm{noise},7}$ to find

$$\underbrace{\sigma_{\mathrm{total},11}-\sigma_{\mathrm{total},7}}_{\text{empirical}}+\underbrace{\sigma_{\mathrm{noise},7}}_{\text{theoretical}} = \underbrace{\sigma_{\mathrm{noise},11}+\underbrace{\left(\sigma_{\mathrm{retrieval},11}-\sigma_{\mathrm{retrieval},7}\right)}_{\text{positive}}}_{B}. \quad (2)$$

$\sigma_{\mathrm{total},11}$ and $\sigma_{\mathrm{total},7}$ are given by the validation results, and $\sigma_{\mathrm{noise},7}$ was modeled. Therefore, the green line B is the 11 GHz SST error due to noise plus the difference in retrieval error, which should usually be positive because the 11 GHz SST retrieval is less accurate, particularly in colder waters. Therefore, as expected, the modeled estimate and B, in Fig. 4(c), are similar in the tropics where there are warmer temperatures. The error B is larger from 40°–60° S and 40°–70° N due to an increase in the 11 GHz retrieval error for cold water. Poleward, B decreases and is less than the modeled estimate of $\sigma_{\mathrm{noise},11}$.

The decrease in error at the highest latitudes is an artifact of the comparison, as shown in Fig. 5. The probability density function of the collocation error (background color), mean bias (solid line), and ± standard deviation (dashed lines) for the 7 GHz [Fig. 5(a)] and 11 GHz [Fig. 5(b)] retrievals show an increase in the standard deviation from 5 °C to 19 °C. This is also seen in Fig. 5(c) which compares the standard deviation for the 7 and 11 GHz retrievals. The AMSR-E and Reynolds SST data minimum value is −1.8 °C, which is the freezing point of sea water. Fig. 5(a) and (b) shows a decreasing bias and standard deviation below 7 °C because the number of large positive differences (AMSR-E minus Reynolds) steadily decreases due to the −1.8 °C minimum temperature. For example, Reynolds is usually within 8 °C of AMSR-E. At an AMSR 11 GHz SST of 10 °C, the possible Reynolds SSTs would be from 2 °C to 18 °C, a spread of 16 °C. At an AMSR 11 GHz SST of 0 °C, the possible Reynolds SSTs would be from −1.8 °C to 8 °C, a spread of 9.8 °C. The −1.8 °C minimum temperature is skewing the results toward a negative bias and a lower standard deviation. This explains the reduction at high latitudes seen in Figs. 3 and 4.

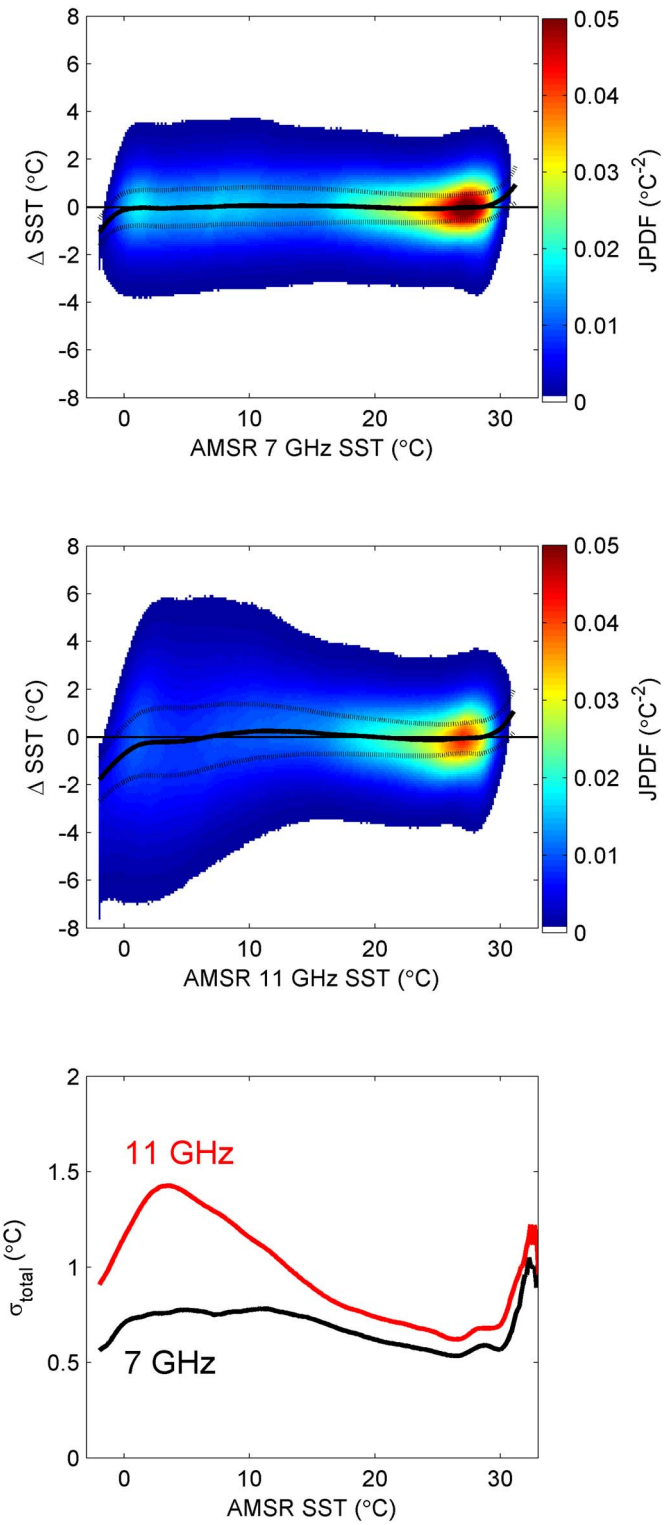

Fig. 5. AMSR-E minus Reynolds SST ΔSST as a function of AMSR-E (a) 7 GHz SSTs and (b) 11 GHz SSTs and (c) the standard deviation of ΔSST as a function of AMSR-E SST.

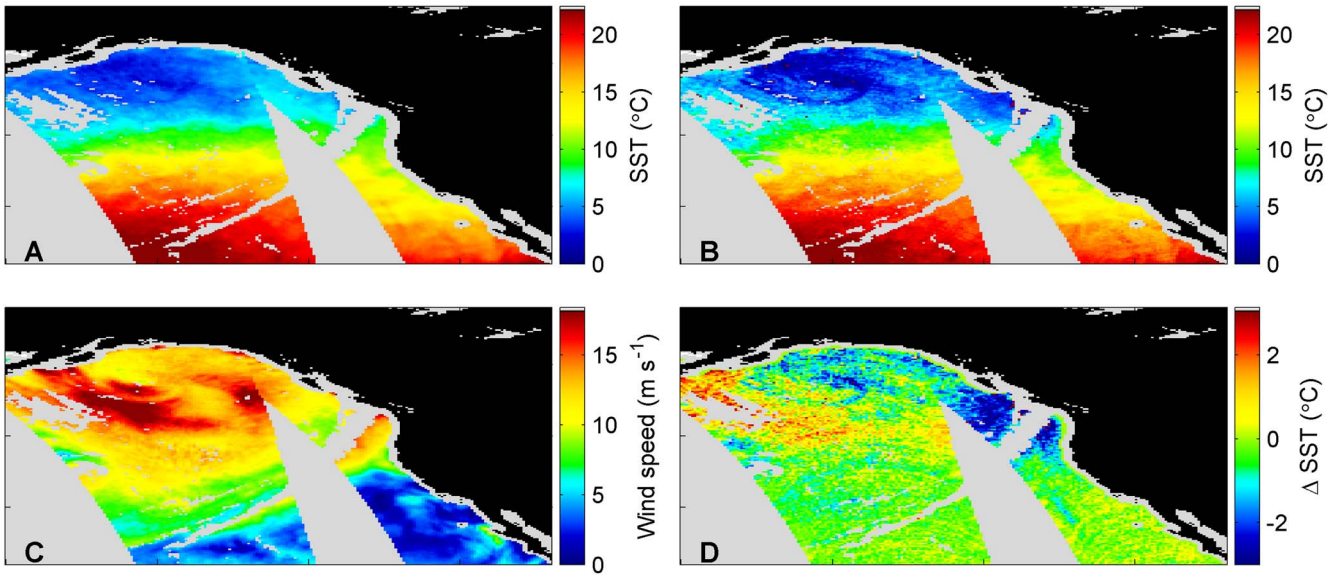

Fig. 6. January 1, 2008 AMSR-E retrievals of (a) 7 GHz SSTs, (b) 11 GHz SSTs, (c) wind speed, and (d) 11 GHz minus 7 GHz SSTs.

The larger error seen at the midlatitudes in Fig. 4, attributed to retrieval error, is shown in Fig. 6. The 7 GHz SST [Fig. 6(a)] is clearly less noisy than the 11 GHz SST [Fig. 6(b)]. There is a visible "swirl" feature south of Alaska in the 11 GHz SST that is less obvious in the 7 GHz SST. This feature can be seen in the AMSR-E wind speed retrievals [Fig. 6(c)] and the difference (7 minus 11 GHz) SSTs. The 11 GHz SST retrieval is not performing as well as the 7 GHz retrieval over cold water with high wind speeds. These wind features are common from $40°-60°$ N−S in both hemispheres and may account for a portion of the increased error shown in Fig. 5.

The sensitivity of the 7 and 11 GHz SST retrieval errors to wind speed is shown in Fig. 7. Retrieval dependences on other atmospheric or oceanic variables are commonly referred to as crosstalk. Ideally, the SST retrievals should not depend on other variables, unless there is a geophysical relationship. Yet, it is very difficult to perfectly remove the effect of oceanic and atmospheric variables on the brightness temperatures, and small dependences exist, which are amplified when the sensitivity to SST is reduced (such as for 11 GHz retrievals of colder water). Fig. 7(a) and (b) shows the 7 and 11 GHz SST retrievals as a function of wind speed (x-axis) and SST (line color). The error is smallest at warmer temperatures for both retrievals. The 7 GHz retrieval error increases (from 0.5 °C to 0.7 °C) at wind speeds greater than 10 $\mathrm{m \cdot s^{-1}}$ for SSTs greater than 20 °C. The error increases as the temperature diminishes, but below 20 °C, the retrieval error does not show a dependence on wind speed (it is constant for all wind speeds). In contrast, the 11 GHz retrieval has a strong dependence on wind speed for all SSTs. The overall error increases as the temperature diminishes and has a larger magnitude than the 7 GHz retrievals. At the lowest SSTs (dark blue lines), the error diminishes because of the SST cutoff effect discussed previously. This sensitivity study shows that the 11 GHz SSTs have larger errors and more dependences on wind speed than the 7 GHz SSTs. This result is specific for SST retrievals based on RTM simulations, regional regression algorithms, or other algorithm formulations may decrease the error due to wind speed.

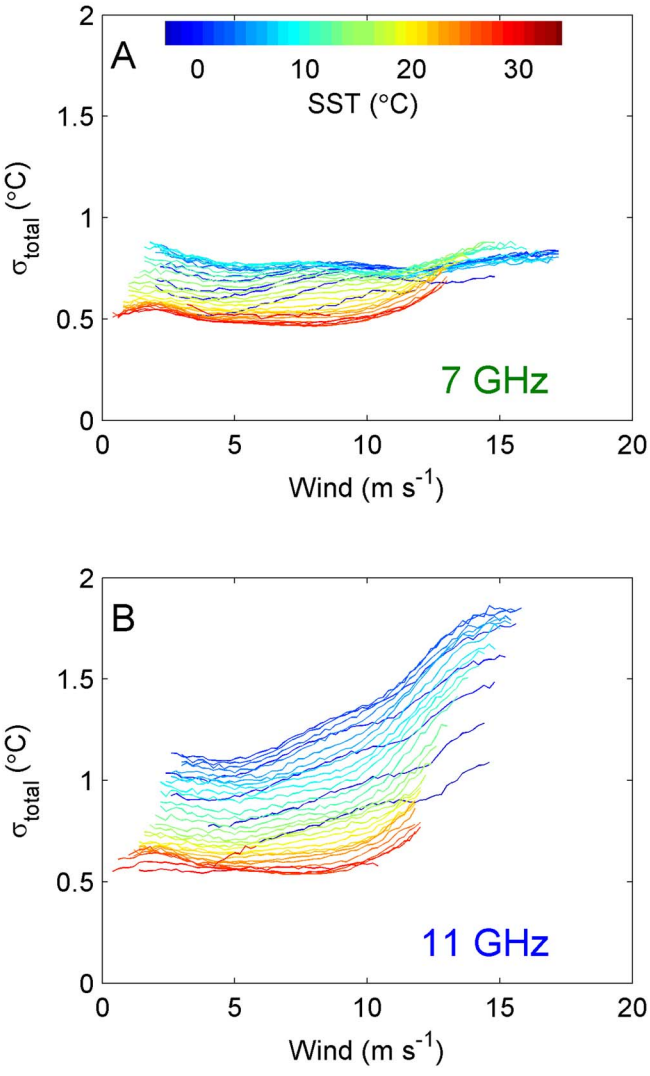

Fig. 7. Standard deviation of AMSR-E minus Reynolds SST ΔSST for the 7 and 11 GHz retrievals as a function of SST and wind speed. SST is shown by the line color while wind speed is given on the x-axis.

V. Conclusion

The 7 GHz SST retrievals have lesser errors due to radiometer noise and geophysical errors than the 11 GHz retrievals at all latitudes. The error for the 11 GHz SST retrieval increases poleward to 40° N−S. In defining future missions, although the addition of a 7 GHz feedhorn to a radiometer is costly, the polar regions are increasingly important areas to monitor for environmental changes, and the use of 7 GHz would provide more accurate SST retrievals. Additionally, while averaging the 11 GHz retrievals will diminish error due to uncorrelated radiometer noise, the geophysical error is still higher than for the 7 GHz retrievals, particularly at the higher latitudes. The success of the TMI microwave SST retrievals is partly due to its limited latitudinal extent, measuring between 40° N−S. The GMI will have larger errors with its expanded orbit measuring between 65° N−S and would therefore benefit from 7 GHz measurements. Of course, future GMI errors will depend not only on the available channels but also on the instrument calibration and retrieval algorithm.

Acknowledgment

The PF Erosion Climatology was downloaded from NASA's Physical Oceanography Distributed Active Archive Center. The Reynolds Optimum Interpolation SST v2 was downloaded from NOAA's National Weather Service Environmental Modeling Center. The AMSR-E SSTs are from Remote Sensing Systems, processed using the version 5 algorithm, and available at www.remss.com.

References

[1] D. B. Chelton and F. J. Wentz, "Global microwave satellite observations of sea surface temperature for numerical weather prediction and climate research," *Bull. Amer. Meteorol. Soc.*, vol. 86, no. 8, pp. 1097–1115, Aug. 2005.

[2] F. J. Wentz, C. L. Gentemann, D. K. Smith, and D. B. Chelton, "Satellite measurements of sea surface temperature through clouds," *Science*, vol. 288, no. 5467, pp. 847–850, May 2000.

[3] D. B. Chelton, F. J. Wentz, C. L. Gentemann, R. A. D. Szoeke, and M. G. Schlax, "Satellite microwave SST observations of transequatorial tropical instability waves," *Geophys. Res. Lett.*, vol. 27, no. 9, pp. 1239–1242, May 2000.

[4] D. B. Chelton, S. K. Esbensen, M. G. Schlax, N. Thum, M. H. Freilich, F. J. Wentz, C. L. Gentemann, M. J. McPhaden, and P. S. Schopf, "Observations of coupling between surface wind stress and sea surface temperature in the eastern tropical Pacific," *J. Clim.*, vol. 14, no. 7, pp. 1479–1498, Apr. 2001.

[5] C. J. Donlon, C. L. Gentemann, and F. J. Wentz, "Measuring surface temperature with microwave sensors," *Backscatter*, vol. 12, no. 2, pp. 37–39, 2001.

[6] C. L. Gentemann, P. J. Minnett, P. Le Borgne, and C. J. Merchant, "Multi-satellite measurements of large diurnal warming events," *Geophys. Res. Lett.*, vol. 35, no. 22, p. L22 602, Nov. 2008.

[7] R. W. Reynolds, C. L. Gentemann, and F. J. Wentz, "Impact of TRMM SSTs on a climate-scale SST analysis," *J. Clim.*, vol. 17, no. 8, pp. 2938–2952, Aug. 2004.

[8] D. Stammer, F. J. Wentz, and C. L. Gentemann, "Validation of microwave sea surface temperature measurements for climate purposes," *J. Clim.*, vol. 16, no. 1, pp. 73–87, Jan. 2003.

[9] C. D. Kummerow, W. Barnes, T. Kozu, J. Shieu, and J. J. Simpson, "The Tropical Rainfall Measuring Mission (TRMM) sensor package," *J. Atmos. Ocean. Technol.*, vol. 15, no. 3, pp. 809–817, Jun. 1998.

[10] J. P. Hollinger and R. C. Lo, "Determination of sea surface temperature with N-ROSS," Naval Res. Lab., Washington, DC, 1984.

[11] F. J. Wentz and T. Meissner, "AMSR ocean algorithm," Remote Sens. Syst., Santa Rosa, CA, 2000.

[12] F. J. Wentz, "A well-calibrated ocean algorithm for Special Sensor Microwave/Imager," *J. Geophys. Res.*, vol. 102, no. C4, pp. 8703–8718, Apr. 1997.

[13] R. W. Reynolds, T. M. Smith, C. Liu, D. B. Chelton, K. S. Casey, and M. G. Schlax, "Daily high-resolution blended analyses for sea surface temperature," *J. Clim.*, vol. 20, no. 22, pp. 5473–5496, Nov. 2007.

[14] K. A. Kilpatrick, G. P. Podestá, and R. Evans, "Overview of the NOAA/NASA Advanced Very High Resolution Radiometer Pathfinder algorithm for sea surface temperature and associated matchup database," *J. Geophys. Res.*, vol. 106, no. C5, pp. 9179–9198, 2001.

[15] C. C. Walton, "Nonlinear multichannel algorithms for estimating sea surface temperature with AVHRR satellite data," *J. Appl. Meteorol.*, vol. 27, no. 2, pp. 115–124, Feb. 1988.

[16] K. S. Casey and P. Cornillon, "A comparison of satellite and *in situ*-based sea surface temperature climatologies," *J. Clim.*, vol. 12, no. 6, pp. 1848–1863, 1999.

[17] R. Evans and G. P. Podestá, *Pathfinder Sea Surface Temperature Algorithm Version 4.0*. Miami, FL: Rosenstiel School Marine Atmos. Sci., Univ. Miami, 1998.

[18] J. D. Jackson, *Classical Electrodynamics*., 3rd ed. New York: Wiley, 1975.

[19] T. Meissner and F. J. Wentz, "The complex dielectric constant of pure and sea water from microwave satellite observations," *IEEE Trans. Geosci. Remote Sens.*, vol. 42, no. 9, pp. 1836–1849, Sep. 2004.

[20] A. Shibata, "Calibration of AMSR-E SST toward a monitoring of global warming," in *Proc. IEEE Int. Geosci. Remote Sens. Symp.*, Seoul, Korea, 2005, vol. 5, pp. 3448–3449.

[21] A. Shibata, "Features of ocean microwave emission changed by wind at 6 GHz," *J. Oceanogr.*, vol. 62, no. 3, pp. 321–330, Jun. 2006.

[22] L. A. Klein and C. T. Swift, "An improved model for the dielectric constant of sea water at microwave frequencies," *IEEE Trans. Antennas Propag.*, vol. AP-25, no. 1, pp. 104–111, Jan. 1977.

Chelle L. Gentemann (M'05) received the B.S. degree in earth, atmospheric, and planetary sciences from the Massachusetts Institute of Technology, Cambridge, in 1995, the M.S. degree in physical oceanography from the Scripps Institution of Oceanography, University of California, La Jolla, in 1997, and the Ph.D. degree in physical oceanography from the Rosenstiel School of Marine and Atmospheric Science, University of Miami, Miami, FL, in 2007.

She has been with Remote Sensing Systems, Santa Rosa, CA, since 1998, working on the retrieval of sea surface temperatures from satellite microwave radiometers, developing physical and empirical models of diurnal warming in the upper ocean, researching the upper ocean response to tropical cyclones, and developing high-resolution blended sea surface temperatures from infrared and microwave radiometers.

Dr. Gentemann is a member of the American Geophysical Union, American Meteorological Society, and IEEE.

Thomas Meissner (M'01) received the B.S. degree in physics from the University of Erlangen-Nürnberg, Nürnberg, Germany, in 1983, the M.S. degree (Diploma) in physics from the University of Bonn, Bonn, Germany, in 1987, and the Ph.D. degree in theoretical physics from the University of Bochum, Bochum, Germany, in 1991. He wrote his doctoral dissertation on effective quark models of the nucleon.

Between 1992 and 1998, he conducted postdoctoral research with the University of Washington, Seattle, the University of South Carolina, Columbia, and Carnegie Mellon University, Pittsburgh, PA, in theoretical nuclear and particle physics, focusing on the theory of strong interaction. Since July 1998, he has been with Remote Sensing Systems, Santa Rosa, CA. Since then, he has been working on the development and refinement of radiative transfer models, calibration, validation, and ocean retrieval algorithms for various microwave instruments (the Special Sensor Microwave Imager, Tropical Rainfall Measuring Mission Microwave Imager, Advanced Microwave Scanning Radiometer—Earth Observing System, WindSat, and Conical Microwave Imager Sounder).

Frank J. Wentz received the B.S. and M.S. degrees in physics from the Massachusetts Institute of Technology, Cambridge, in 1969 and 1971, respectively.

In 1974, he established Remote Sensing Systems (RSS), Santa Rosa, CA, a research company specializing in the satellite microwave remote sensing of the Earth. His research focuses on radiative transfer models that relate satellite observations to geophysical parameters, with the objective of providing reliable geophysical data sets to the Earth Science community. As a member of the National Aeronautics and Space Administration (NASA)'s SeaSat Experiment Team (1978–1982), he pioneered the development of physically based retrieval methods for microwave scatterometers and radiometers. Starting in 1987, he took the lead in providing the worldwide research community with high-quality ocean products derived from satellite microwave imagers [Special Sensor Microwave Imager (SSM/I)]. As the Director of RSS, he overseas the production and validation of reliable scatterometer and radiometer products. These data are dispersed via the company's Web and FTP sites. He is currently a member of the NASA Earth Observation System Investigators Working Group, NASA Advanced Microwave Scanning Radiometer Team, NASA Ocean Vector Wind Science Team, NASA Tropical Rainfall Mission Team, and NASA Pathfinder Activity. He is currently working on scatterometer/radiometer combinations, satellite-derived decadal time series of atmospheric moisture and temperature, the measurement of sea surface temperature through clouds, and advanced microwave sensor designs for climatological studies. He has served on many NASA review panels, the National Research Council's Earth Studies Board, and the National Research Council's Panel on Reconciling Temperature Observations.

Mr. Wentz is a member of the American Geophysical Union.